Stochastic boundary molecular dynamics simulation of L-ribose in the active site of Actinoplanes missouriensis xylose isomerase and its Val135Asn mutant with improved reaction rate

ARTICLE *in* BIOCHIMICA ET BIOPHYSICA ACTA · JUNE 2005

Impact Factor: 4.66 · DOI: 10.1016/j.bbapap.2005.02.007 · Source: PubMed

7 AUTHORS, INCLUDING:

Ossi Pastinen
Aalto University
32 PUBLICATIONS **374** CITATIONS
SEE PROFILE

Matti Leisola
Aalto University
155 PUBLICATIONS **4,342** CITATIONS
SEE PROFILE

Ossi Turunen
Aalto University
60 PUBLICATIONS **2,379** CITATIONS
SEE PROFILE

Available online at www.sciencedirect.com
SCIENCE DIRECT
Biochimica et Biophysica Acta 1749 (2005) 65–73
BIOCHIMICA ET BIOPHYSICA ACTA
BBA
http://www.elsevier.com/locate/bba

Stochastic boundary molecular dynamics simulation of L-ribose in the active site of *Actinoplanes missouriensis* xylose isomerase and its Val135Asn mutant with improved reaction rate

Harri Santa[a,1], Juha Kammonen[a,1], Olli Lehtonen[b], Johanna Karimäki[a], Ossi Pastinen[a], Matti Leisola[a], Ossi Turunen[a,*]

[a]*Laboratory of Bioprocess Engineering, Helsinki University of Technology, P.O. Box 6100, 02015-TKK, Finland*
[b]*Department of Engineering Physics and Mathematics, Helsinki University of Technology, P.O. Box 2200, 02015-TKK, Finland*

Received 11 February 2004; received in revised form 11 February 2005; accepted 14 February 2005
Available online 8 March 2005

Abstract

We used molecular dynamics simulations to study how a non-natural substrate, L-ribose, interacts with the active site of *Actinoplanes missouriensis* xylose isomerase. The simulations showed that L-ribose does not stay liganded in the active site in the same way as D-xylose, in which the oxygens O2 and O4 are liganded to the metal M1. The oxygen O4 of L-ribose moved away from the metal M1 to an upside down position. Furthermore, the distances of the carbons C1 and C2 of L-ribose to the catalytic metal M2 were higher than in the case of D-xylose. These findings explain the extremely low reaction rate of xylose isomerase with L-ribose. The mutation V135N close to the C5–OH of the substrate increased the reaction efficiency 2- to 4-fold with L-ribose. V135N did not affect the reaction with D-xylose and L-arabinose, whereas the reaction with D-glucose was impaired, probably due to a hydrogen bond between Asn-135 and the substrate. When L-ribose was the substrate, Asn-135 formed a hydrogen bond to Glu-181. As a consequence, O4 of L-ribose stayed liganded to the metal M1 in the V135N mutant in molecular dynamics simulations. This explains the decreased K_m of the V135N mutant with L-ribose.

Keywords: Xylose isomerase; L-Ribose; Molecular dynamics; Site-directed mutagenesis; Catalytic efficiency

1. Introduction

Enzymes are highly specific but can often accept a wide variety of substrate-related molecules and many of them are non-natural. This allows a way for a protein engineer to use enzymes for industrially useful reactions by improving the reaction efficiency with the non-natural substrates. Xylose isomerase (XI) catalyzes the interconversion (isomerization) of aldose and ketose sugars. Thus, XI converts D-xylose to D-xylulose and D-glucose to D-fructose [1,2]. XI accepts also other substrates, e.g. D/L-arabinose and D/L-ribose, but with lower efficiency [3]. In addition to isomerization, XI is also able to catalyze C2 epimerization of aldoses [3–6]. Thus, D-xylose is converted to D-lyxose by epimerization. The simplest way to produce the epimer is by double-isomerization, i.e. the conversion of aldose-1 (e.g. D-xylose) first to ketose (D-xylulose) and then to aldose-2 (D-lyxose). When the ketose sugar is used as the substrate it is transformed to both of the aldoses. However, other mechanisms have also been proposed for the epimerization [2,3].

The interactions of the substrate in the xylose isomerase active site and the reaction mechanism have been studied by site-directed mutagenesis, crystallography and computer simulations [1,2,7,8]. The enzyme reaction starts with ring opening and, subsequently, the substrate binds to the active site in a linear form. The oxygens O2 and O4 are liganded to

* Corresponding author. Tel.: +358 9 451 2551; fax: +358 9 462 373.
E-mail address: Ossi.Turunen@hut.fi (O. Turunen).
[1] Both authors contributed equally to this paper.

1570-9639/$ - see front matter © 2005 Elsevier B.V. All rights reserved.
doi:10.1016/j.bbapap.2005.02.007

the structural metal M1 that is usually Mg^{2+} or Mn^{2+}. When an aldose sugar is the substrate, the enzyme reaction starts with a proton transfer leading to the loss of proton from oxygen O2. In the next steps, a hydride shift occurs from carbon C2 to C1. Concomitantly with the hydride shift, the catalytic metal M2 moves from a more distant position closer to the substrate and becomes coordinated to the oxygens O1 and O2. Initially, Lys-183 (*Actinoplanes missouriensis* XI numbering) forms a hydrogen bond to O1 and keeps the oxygen O1 in a conformation, which allows liganding of the metal M2 to the substrate [9–11]. During the hydride shift the conformation of the dihedral angle O2–C2–C1–O1 is close to zero [7,11,12].

We have used site-directed mutagenesis to study how to improve the reaction of XI with non-natural substrates. Here we report molecular dynamics simulation analysis of the interactions of L-ribose in the active site of XI and the improvement of the reaction rate by a mutation near the oxygen O5 of the substrate.

2. Materials and methods

2.1. Production of xylose isomerases

XI was cloned from *A. missouriensis* by polymerase chain reaction (PCR) into pQE60 expression vector (Qiagen) between Nco I and *Hin*dIII sites. The site-directed mutagenesis was performed by PCR as described earlier [13]. Swiss-PdbViewer [14] was used in mutation planning. *E. coli* XL1 Blue cells (Stratagene) were used to express XI; the production was induced by 1 mM IPTG. The enzyme purification was done in the following way: the cells containing XI were disrupted by sonication in 0.2 M maleic acid/20 mM $MgSO_4$/1 mM $CoCl_2$ buffer (pH 7), the *E. coli* proteins in the supernatant were removed by heat precipitation (15 min, 60 °C) and XI was finally purified by cation exchange chromatography (DEAE–Sepharose FastFlow; Amersham-Pharmacia). The chromatography buffer was 0.05 M sodium acetate (pH 5.8) containing 0.01 M $MgCl_2$. The proteins were eluted from the column by 0–1.0 M NaCl gradient in the chromatography buffer. The XI sample was dialyzed to the reaction buffer (see below). The enzyme samples were concentrated by a centrifugal filter device (Millipore Centriprep, Amicon Bioseparations). The protein concentration was measured using the Bio-Rad method, which is based on Bradford's method [15], using bovine serum albumin (Sigma) as standard.

2.2. Xylose isomerase assay

XI activity with different substrates was measured by incubating the enzyme and substrate in 50 mM TEA/10 mM Mg_2SO_4 buffer (pH 7.5) for various lengths of time at 60 °C. The substrates were D-glucose, D-xylose, L-arabinose and L-ribose. The reaction was stopped by adding 1 M H_2SO_4 (final concentration 0.1 M) and the amount of sugars was measured by HPLC using an Aminex HPX-87P column (Bio-Rad). When measuring the time-dependent activity curves, the substrate concentration was 30 g/l. Enzyme concentrations were 0.2 g/l with D-xylose, 0.5 g/l with D-glucose and 2.0 g/l with L-arabinose and L-ribose. For the determination of K_m and k_{cat}, concentration ranges of 237.5–12.5 g/l of D-glucose and 225–25 g/l of L-ribose were used. The enzyme concentrations used were 0.5 g/l for D-glucose and 1.0 g/l for L-ribose. The kinetic parameters were calculated using Dynafit [16] and Lineweaver–Burke's plot (the results were also confirmed using the Eadie–Hofstee plot).

2.3. Modeling of the V135N mutant

The structure of the mutant was modeled initially by using Quanta software (version 2000) [17]. The starting structure was the structure of *A. missouriensis* XI (PDB code 6XIM [18]). Water molecules, two magnesium atoms as well as the substrate (D-xylose) were removed from the coordinate file. Then the side chain conformations were modeled by grid search under the conformational search module of Quanta. In the grid search, two essential side chain dihedral angles were rotated in steps of 15°, followed by energy minimization and energy estimation. The resulting optimum conformation of Asn at position 135 had a value of about 178° for the dihedral angle N–CA–CB–CG and a value of 40° for the dihedral angle CA–CB–CG–OD1.

2.4. Molecular dynamics simulations

The stochastic boundary molecular dynamics simulation [19,20] was used to study L-ribose in the active site of the dimeric form of *A. missouriensis* XI (6XIM). The dimer was prepared from tetramer by removing two subunits. Thus, the essential Phe-26 coming from the other subunit into the active site, and being important for the activity, was included in the simulations. L-Ribose and D-xylose were modeled in linear forms into the active site of XI. The program CHARMM (versions 27 and 28) was used with all-atoms MSI CHARMm force fields in the calculations, namely, AMINOH.RTF and PARM.PRM, which are the topology file and parameter file, respectively, for CHARMm version 22 [21,22]. Hydrogen atoms were built by HBUILD [23]. The solvent molecules were built to surround the protein structure and then removed if they were located outside the region of 24 Å from the carbon C2 of substrate. TIP3 was used for the water model [24]. The reaction region was a sphere of 13.0 Å from the carbon C2. The buffer region was defined as the region between the distance 13.0 and 15.0 Å from the carbon C2. A frictional coefficient of 62 ps^{-1} was placed on all oxygens of water molecules. An average friction coefficient of 250 ps^{-1} was used for protein atoms in the buffer region. A spherical boundary potential was used to prevent the water molecules

escaping into vacuum. TIP3P deformable boundary forces computed for a 16.8 Å sphere were used. The SHAKE algorithm [25] was used to constrain all bonds to their equilibrium values with the tolerance value of 1×10^{-6}. A force shifting function was used to cut off the Coulombic term at 12 Å and a shifting function was used to cut off the van der Waals term at 12 Å, as recommended by CHARMM documentation and Steinbach and Brooks [26]. A time step 2 fs was used and the non-bonded list was updated in every 20 steps based on 13 Å list cutoff distance. The simulation lengths were 400 ps. The atoms in the buffer region were treated by Langevin dynamics. Simulations were performed at 333 K.

In the starting structure of simulations, O2 and O4 were constrained close to the metal M1 using a distance constraint of 2.4 Å between metals and oxygens. The distance between the metals was constrained close to 4.6 Å, a distance similar to that in 6XIM. Without the constraint the metal M2 tended to move. Often, the dihedral angle O2–C2–C1–O1 was constrained to *cis*-conformation. In the final simulation, the magnesium atoms were kept fixed. The charges of the side chain (–CH2–NH3) of Lys-183 and metal M2 were varied. The charge of metal M1 was often set to +2.0. This may not be exactly correct since a decrease in the charges arises from the electronic flow from surrounding acidic groups. However, it was practical to use the charge of +2.0 for metal M1 to keep O4 and O2 atoms in its vicinity in reference simulations with D-xylose. The same charges that exist for D-xylose in the modified CHARMM topology file (software CRATE-version 9.0; [27]) were used for D-xylose with minor modifications. The charge value of −0.45 was used for the O1 atom of D-xylose in most simulations. This allowed a slightly weaker interaction with metals than the value of −0.671 in CRATE 9.0 [27].

The charges used for L-ribose in the simulations were estimated by a combined quantum mechanical/molecular mechanical method [28] using PM3 semi-empirical calculations [29] and Mulliken population analysis [30] for the substrate. In the method, only substrate was handled by quantum mechanics and other groups were by molecular mechanics. The calculations were performed in a stochastic boundary molecular dynamics environment. The starting structure was created using MD, followed by steepest descent energy minimization. In the calculations, template based MM-charges [22] for L-ribose created by Quanta were used and oxygens O2 and O4 of the substrate were constrained close to the metal M1. Finally, the structure of L-ribose was described by PM3 [29] and it was optimized by steepest descent algorithm using 20,000 steps. The atoms O2 and O4 were kept fixed. The resulting charges for L-ribose were 0.289 (C1), 0.167 (C2), 0.004 (C3), 0.029 (C4), 0.031(C5), −0.432 (O1), −0.960 (O2), −0.433 (O3), −0.398 (O4), −0.362 (O5), 0.055 (H1), −0.018 (H2), 0.053 (H3), 0.089 (H4), 0.042 (H5), 0.062 (H6), 0.282 (HO1), 0.277 (HO2) and 0.221 (HO3).

Asp-257 was in the protonated form or in some simulations in unprotonated form; p*K*a calculations by WHATIF/Delphi [31,32] proposed its p*K*a value to be about 7 in the monomeric apo form without metals and the substrate. All histidines were uncharged with a proton on ND1.

In the simulations of L-ribose, NE2 atom of His-220, OD1 atom of Asp-255 and OD1 atom of Asp-257 were constrained to bind to the catalytic magnesium and in the final simulations they were kept fixed. During the simulation, the OE2 atom of Glu-217 was constrained to stay in contact with metal M2. OD2 atom of Asp-292 was fixed to stay in a position close to metal M. The distance of the NE2 atom of His-220 from Mg2 was about 2.5 Å, similar to the distance in the crystal structure of XI complexed with L-arabinose [33]. The distance of the OD1 atom from Mg2 was less than 2.2 and 2.3 Å for Asp-255 and Asp-257, respectively. Asp-257 was modeled in these simulations to be in unprotonated form because it interacts with the metal M2.

D-xylose was simulated in the structure of 6XIM. The distance of the OD2 atom of Asp-255 from the metal M2 was about 2.7–2.8 Å and the OD1 atom of Asp-257 was modeled to be 2.9–3.1 Å away from the metal M2. In the final simulations, OD2 atom of Asp-255, OD1 atom of Asp-257, OE2 atom of Glu-217, NE2 atom of His-220 and OD2 atom of Asp-292 were kept fixed. This enabled the comparison of the crystal structure and the modeled structure of D-xylose. In the simulations, charges of the NH3-group of Lys-183 and metal M2 were varied. The simulations were performed using two different protonation states for Asp-257.

2.5. Quantum chemical calculations

Quantum chemical calculations were done with 6XIM and the crystal structure of *S. rubiginosus* XI complexed with L-arabinose [33]. Side chains were truncated and modified by adding missing hydrogens. The size of the active site models (based on 6XIM) were 219 atoms including D-xylose and Asp-257 in the unprotonated form, or 200 atoms with Asp-257 in protonated form. These model structures had the net charge of −1. The model with 219 atoms consisted of the side chains of Trp-16, Lys-183, Glu-186, Pro-187, His-220, Glu-217, His-54, Glu-181, His-220, Asp-245, Asn-247, Asp-255, Asp-257, Lys-294 and Phe-26 as well as D-xylose, both Mg atoms and seven water molecules. The model with 200 atoms consisted of the side chains of Trp-16, Lys-183, Glu-186, Pro-187, His-220, Glu-217, His-54, Glu-181, His-220, Asp-255, AspH-257, Lys-294 and Phe-26 as well as D-xylose, both Mg atoms and six water molecules. The positions of water molecules were adjusted by stochastic boundary molecular dynamics and by the energy minimization of the structure. An active site model with 137 atoms was also created based on the crystal structure of XI complexed with L-arabinose [33]. This model structure had the net charge of −2. In the model,

Asp-257 was in unprotonated form. The side chains of Trp-16, Lys-183, Glu-186, Pro-187, His-220, Glu-217, Asp-255, Asp-257 and Met-88 were represented in the model as well as Mg2 atom and L-arabinose in a singly negatively charged form. There were no water molecules in this calculation. The Mulliken [30] population analysis was made by performing single point energy calculation using density functional theory with BLYP functional [34,35] and a standard split-valence (SV(P)) basis set including polarization functions in all non-hydrogen atoms. Calculations were made with TURBOMOLE program employing the resolution of the identity approximation of the Coulomb interaction [36,37].

3. Results

3.1. Effect of V135N on reaction efficiency

The wild type *A. missouriensis* XI and the mutant V135N enzymes were produced intracellularly in *E. coli* and purified by heat precipitation and cation exchange chromatography. The proteins were over 95% pure when estimated in SDS-PAGE (data not shown). The mutant enzyme was compared to the wild type by following the time course of enzyme reaction and determining the K_m and k_{cat} parameters. The enzyme assay with different substrates showed that the mutation V135N improved the reaction of XI only with L-ribose.

L-ribose is converted by XI first to L-ribulose and then to L-arabinose (C2 epimer of L-ribose) (Fig. 1). Correspondingly, L-arabinose is converted to L-ribulose and L-ribose in the reverse reaction. The initial velocity of the enzyme reaction with L-ribose was higher with the V135N mutant than that of the wild type XI (Fig. 2). The conversion rate of L-ribose into L-arabinose was improved 4-fold, whereas the improvement for the conversion of L-ribose to L-ribulose was 1.8-fold (Fig. 2; Table 1). When L-arabinose was used as the substrate, the V135N mutation did not change the reaction rate of XI from the wild type level (Table 1). This showed that the improvement of the reaction efficiency with L-ribose was a specific property of the V135N mutant. The V135N mutation decreased the reaction rate with D-glucose substantially, whereas the reaction rate with D-xylose remained quite close to the wild type level (Table 1).

3.2. Kinetic parameters

The mutation V135N lowered the K_m value for D-glucose to about 35% from that of the wild type XI (Table 2). However, at the same time k_{cat} was lowered to 13% from that of the wild type. Thus, the catalytic efficiency of the V135N mutant with D-glucose was 2.6-fold smaller compared to the wild type XI (Table 2).

When L-ribose was the substrate, a significant amount of L-arabinose was produced early in the reaction almost at the same time as L-ribulose (Fig. 2). Therefore, the kinetic parameters were determined so that the product of the enzyme reaction was the sum of the produced L-ribose and L-arabinose. The V135N mutation mainly affected the K_m value. K_m became 3-fold lower due to the mutation V135N, whereas k_{cat} was decreased only slightly (Table 2). Consequently, the catalytic efficiency of the mutant was 2.7 times higher than that of the wild type.

3.3. Polarization effect and simulation of D-xylose in the active site of XI

CHARMM force field provided by Accelrys Inc. [21,22] did not take into account the polarization effect [38]. Thus, charges of atoms in the active site may differ from those in the force field. Quantum chemical calculation was therefore used to estimate the charges for atoms in the active site. The obtained charges were lower for some essential atoms than in the CHARMM force field. For example, the charge of the NH3-group of Lys-183 was calculated to be +0.50, +0.58 and +0.58 in the three different active site models (137-, 200- and 219-atoms models, respectively) in contrast to +0.75 in the CHARMM force field. Furthermore, we calculated the charges of the metals to be in the range of +1.0–+1.1 instead of +2.0. Also, the negative charges of those COO-groups, which contact with metals, were

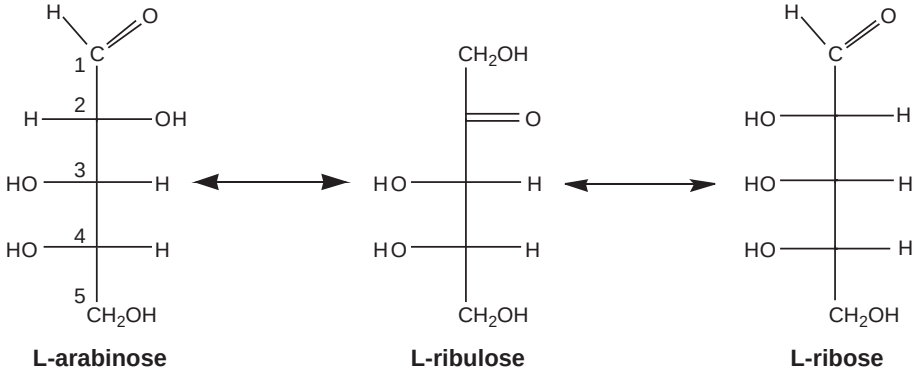

Fig. 1. Schematic structures of arabinose, ribulose and ribose. The numbering of sugar carbons is shown for arabinose.

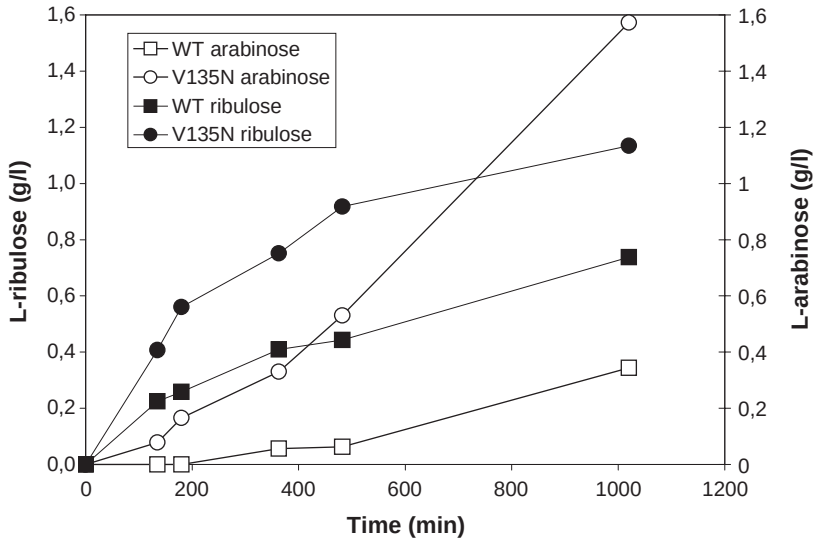

Fig. 2. Initial velocities of *A. missouriensis* XI and the V135N mutant with L-ribose as substrate.

lowered by about 0.4 units and being about −0.60 in contrast to −1.0 in CHARMM. The charge of the NH3-group of Lys-294 was also estimated to be less than +0.50 in the models. The charges for the O1, C1, H1 and O2 atoms of the substrate were estimated to vary in the range of −0.19–0.28, 0–0.46, −0.04–0.10 and −0.50–0.71, respectively. Thus, the three active site models gave quite similar values for these atoms, except for C1, in which the 137 atoms model gave a deviating value (the charge was 0).

The strength of the contacts between the metal M2 and the side chains around it was artificial and lowered since we often used a charge that was less than +1 for M2 instead of the MM-charge that is +2.0. In long simulations, a low charge of M2 could lead to the disappearance of important contacts, thereby causing conformational changes in the side chains close to the metal M2. However, our aim was to keep the structure of the protein similar to the crystal structure during the simulation and, therefore, structural constraints were often needed.

The molecular dynamics simulations of D-xylose using different charge combinations revealed that the distance of the O1 atom of the substrate from the NH3-group of Lys-183 varied in a charge-dependent way (Table 3). The inspection of the simulated structures revealed that the NH3-group was in some cases able to populate a different conformation than in the crystal structure. In particular, this happened when the charges were too high for the NH3-group of Lys-183 or metal M2. In these structures, the NH3-group interacted more with the CO-group of the backbone of Glu-186, which is located behind the NH3-group of Lys-183 with respect to the substrate O1 atom. In conclusion, the deviation from the *cis*-conformation of the O2–C2–C1–O1 dihedral angle appeared to depend on the set of the charge values of the metal M2 and NH3-group of Lys-183. We observed that the charges of the metal M2 and NH3-group of Lys-183 lower than estimated by quantum chemical calculations gave conformations of D-xylose similar to that in the crystal structures (Table 3).

Asp-257 takes part in the proton shuttling before the hydride shift occurs and is likely to be both in unprotonated and protonated form during the proton shuttling (see [1]). In crystal structures, O1 of the substrate is not in *cis*-conformation with O2, probably due to the hydrogen bond to Lys-183. A charge combination, giving a simulated structure closest to the crystal structure (6XIM), was +0.6 for the catalytic magnesium (metal M2) and +0.6 for the NH3-group of Lys-183, when Asp-257 was in the unprotonated form (Table 3). As a result, the NH3-group of Lys-183 was located in the vicinity of O1 atom of the substrate (D-xylose) and the deviation of 51° from the *cis*-conformation of O1 and O2 is close to the same as in the crystal structure

Table 1
Initial velocities of *A. missouriensis* XI and the V135N mutant with different substrates

Reaction	Wild type	V135N
D-glucose to D-fructose (mg/g/s)	28	6.4
D-xylose to D-xylulose (mg/g/s)	97	82
L-arabinose to L-ribulose (mg/g/h)	430	400
L-arabinose to L-ribose (mg/g/h)	38	46
L-ribose to L-arabinose (mg/g/h)	14	57
L-ribose to L-ribulose (mg/g/h)	50	91

The formation of the product is expressed in milligrams per gram enzyme in a second or hour, respectively.

Table 2
Kinetic parameters of *A. missouriensis* XI and the V135N mutant for D-glucose and L-ribose

Substrate		K_m (mM)	k_{cat} (1/s)	k_{cat}/K_m ratio to WT
D-glucose	Wild type	713	26.3	1
	V135N	244	3.47	0.39
L-ribose	Wild type	1312	2.52×10^{-2}	1
	V135N	438	2.26×10^{-2}	2.69

Table 3
Average distances (dist) of the substrate oxygen O1 to the nitrogen atom of the side chain of Lys-183 and average dihedral angle O2–C2–C1–O1 (dihe) values of the substrate obtained from the simulations

	Dist (Å)	Dihe (°)
D-Xylose		
+0.39 (Mg:+1.1)[a]	5.0	−18.6
+0.39 (Mg:+0.6)[a]	3.1	−33.5
+0.60 (Mg:+0.6)[a]	2.8	−51.1
+0.60 (Mg:+1.1)[a]	4.5	−15.4
+0.39 (Mg:+0.6)[b]	3.3	−27.6
+0.60 (Mg:+0.6)[b]	3.7	−25.6
+0.39 (Mg2:1.0)[b]	3.8	−20.0
+0.48 (Mg2, Mg1:1.1, 1.2 O1:−0.61)[b]	3.9	−9.7
+0.39 (O1:−0.671)[b]	5.1	−0.5
+0.60 (Mg2:1.0, E186:−0.60, D253:−0.60)[b]	5.2	−17.0
+0.60 (Mg2:+0.6, E186:−0.60, D253:−0.60)[b]	5.2	−17.8
+0.39 (Mg2:+0.6, E186:−0.60, D253:−0.60)[b]	4.0	−23.5
Crystal structure (6XIM)	3.0	−34, −48

The results are presented as a function of the charges of NH3-group of Lys-183 and other modified charges (in parenthesis). We used charge of zero for the CH2-group in all simulations. The 400 ps simulations were performed at 333 K. For default charges and other details, see Materials and methods.
[a] Asp-257 was in unprotonated form.
[b] Asp-257 was in protonated form.

(6XIM) (Table 3). Also, the distance between O1 atom of D-xylose and the NH3-atom of Lys-183 was 2.8 Å, which is very similar to the crystal structures 6XIM and 3XIS. Furthermore, the charge of +0.39 for the NH3-group of Lys-183 gave results also close to the crystal structure (6XIM). When Asp-257 was in a protonated form the best result was achieved with the charges of +0.6 and +0.39 for the metal M1 and NH3-group of Lys-183, respectively. However, the deviation from *cis*-conformation of O2 and O1 was not as high as in the simulation with the unprotonated form of Asp-257. It can be concluded that SBMD simulations suggested that the charges could be even lower, at least for the metal M2, than what were derived from the quantum chemical calculations.

In the reference simulation with D-xylose, the oxygen O4 atom and the whole substrate were positioned quite similarly than what is seen in the crystal structure (6XIM), including the simulations shown in Fig. 3. Thus, the charges of the metal M2 and the NH3-group of Lys-183 did not affect the stability of the contact between the oxygen O4 of D-xylose and the metal M1.

3.4. L-ribose in the active site of XI

The structure of L-ribose in the active site of *A. missouriensis* XI was modeled by CHARMM. Initially, oxygens O2 and O4 of L-ribose were fixed to be liganded to the metal M1 (distance limit 2.4 Å) in a similar way than O2 and O4 of D-xylose (6XIM) and then the substrate was simulated by molecular dynamics. During the course of simulation, O4 of L-ribose started to move away from liganding to the metal M1 and O3 moved to become bound directly to M1. In an intermediate stage, O4 was located on

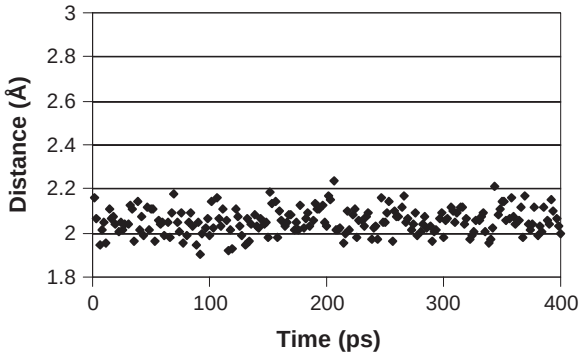

Fig. 3. Simulation of the reactive open chain form of D-xylose. The time series shows the distance between the O4 atom and the structural magnesium (M1) during the simulation. The figure presents simulations with the charges of +2.0, +0.6 and +0.60 for the metals M1 and M2 and the NH3-group of Lys-183, respectively.

the side of the side chain of Glu-181. The movement of O4 appeared to be strengthened by the repulsive interaction of O4 with the carbonyl oxygen of Glu-181 (the side chain of Glu-181 is liganded to the metal M1). At the end of a very short simulation or even immediately after the preceding structure optimization by steepest descent algorithm, O4 was located upside down with respect to the starting conformation (Fig. 4). This conformation was stable during 400 ps in the simulation (Fig. 5). The same results were obtained even when some of the essential charges were varied (Fig. 5). On the contrary, when D-xylose was modeled to be liganded to M1, the substrate did not move away from its place during the simulation with similar parameters (Fig. 3).

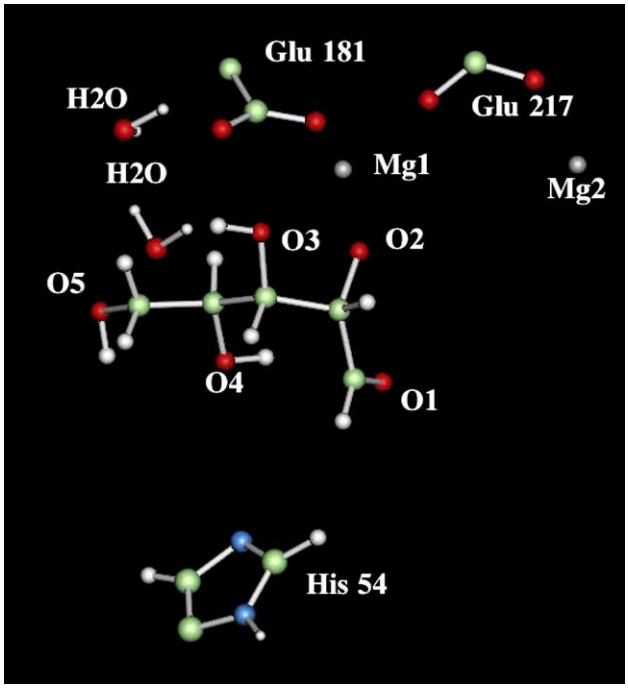

Fig. 4. Modeled structure of L-ribose in the active site of *A. missouriensis* XI. The model presents a snapshot from the molecular dynamics simulations of the wild type XI liganded with L-ribose.

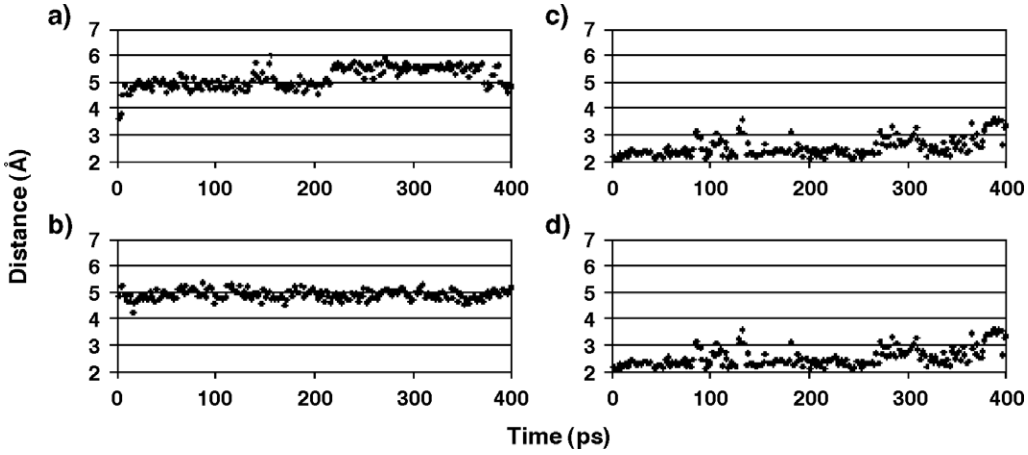

Fig. 5. Time series for the contact between O4 atom of the substrate and the structural metal M1 in the simulations of L-ribose in the active site of the wild type XI (a, b) and the V135N mutant (c, d). In the simulations a and c, the charge of the NH3-group of Lys-183 was set to +0.39 and the charge of the metal M2 was set to +0.7. In the simulations b and d, these charges were set to +0.60 and +1.1, respectively.

In some simulations the HO4 atom of L-ribose was able to form a hydrogen bond with the NE2 atom of His-54. In others, the HO4 atom was not constantly hydrogen bonded to His-54 (Fig. 4). In the latter simulations, we used charges lowered by 0.21 units for the NH3-group of Lys-294 to weaken its interaction with the substrate (otherwise Lys-294 may interact with O1 of the substrate). According to quantum chemical studies these results would be closer to reality. The charge of the NH3-group of Lys-294 was estimated by quantum chemical calculation to be +0.5 or even lower as compared to the value of +0.75 in the parameters of CHARMM force field.

The residue Val-135 is located close to the oxygen O5 of the pentose substrate in the active site of *A. missouriensis* XI. In the SBMD simulation, in which Val-135 was mutated to Asn and the side chain of Asn-135 was hydrogen bonded to Glu-181, there was no relocation of the O4 atom from liganding to the metal M1 during the simulation of 400 ps, even when the active site parameters were varied (Fig. 5). The substrate remained in a conformation shown in Fig. 6. In contrast to the wild type simulations, the HO5 atom hydrogen bonded to the NE2 atom of His-54 in the V135N mutant. One water molecule interacted in the simulations of the V135N mutant with the O4 atom of L-ribose and the NH2-group of N135 and COO-group of E181. This water molecule may have an influence on the stability of the substrate conformation. It stayed during the whole simulation in its place (Fig. 6).

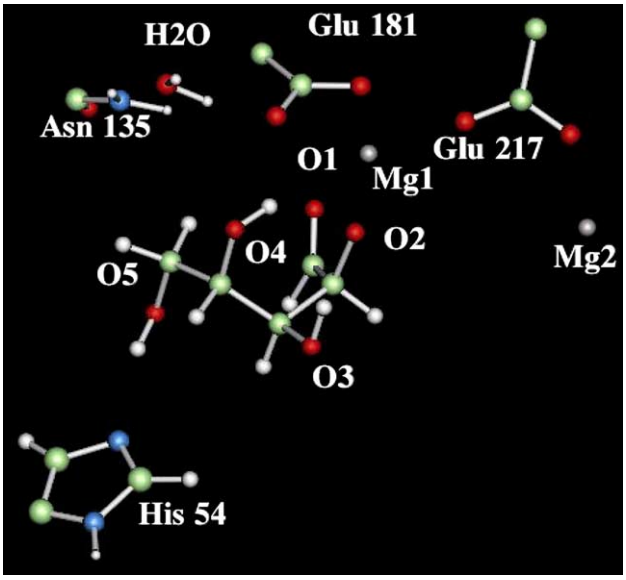

Fig. 6. Modeled effect of the V135N mutation. The model presents a snapshot from the molecular dynamics simulations of the mutant enzyme liganded with L-ribose.

We also studied how the mutation V135N affects the distance between the catalytic metal M2 and the C2–C1 region of the substrate. The reference distances are 3.86 Å for C2–M2 and 3.54 Å for C1–M2 in XI complexed with D-xylose (6XIM). Similar results were achieved also using molecular dynamics: the obtained values were 4.0–4.2 Å (C2–M2) and 3.4–3.8 Å (C1–M2) depending on the used charge combination (Table 4). The corresponding distances were 5.9 Å (C2–M2) and 6.2 Å (C1–M2) for simulated L-ribose. In our simulations, the position of L-ribose in the

Table 4
Average distances (Å) of the substrate carbons C1 and C2 to the catalytic metal M2

	C1–M2	C2–M2
D-Xylose (6XIM)	3.54	3.86
D-Xylose (MD of 6XIM)	3.4–3.8	4.0–4.2
L-Ribose-a	6.2	5.9
L-Ribose-b	6.1	5.9
L-Ribose (V135N)-a	5.9	5.2
L-Ribose (V135N)-b	5.6	4.8

The values for L-ribose were calculated from MD simulation trajectories and values for D-xylose were calculated from 6XIM or MD simulation trajectories of 6XIM (Table 3). a) The charges of the metals M1 and M2 and the NH3-group of Lys-183 were set to +2.0, +0.7 and +0.39, respectively. b) The charges of the metals M1 and M2 and the NH3-group of Lys-183 were set to +2.0, +1.1 and +0.6, respectively.

active site was not very sensitive to the changes in the charges of the metal M2 and Lys-183. In conclusion, the simulations showed that the C1 and C2 carbons of L-ribose have a longer distance to the catalytic metal M2 than the same atoms of D-xylose in the crystal structure (6XIM) (Table 4). The mutation V135N shortened the distances of the C1 and C2 carbons to the metal M2 by 0.4–0.9 Å (Table 4).

4. Discussion

Crystal structures of the enzyme–substrate complexes for substrates showing a lower reaction rate with XI may reveal reasons why the enzyme does not react efficiently with them. However, it may be difficult to determine crystal structures for substrates that are not favored in the reaction equilibrium. For example, in the reactions of L-ribose, L-ribulose and L-arabinose by XI (Fig. 1), the reaction equilibrium favors the formation of L-arabinose. When studied with *S. rubiginosus* XI, the equilibrium concentration is 80% for L-arabinose at 25 °C and for L-ribose it is 17% [3]. The reaction of XI with L-ribose is very slow. For *S. rubiginosus* XI, the reaction with L-ribose is 20 times slower than with L-arabinose and 2500 times slower than with D-glucose [3].

Therefore, we analyzed the structure of L-ribose in the active site of *A. missouriensis* XI by modeling with CHARMM. The modeled structure indicated some reasons for the low reaction efficiency of XI with L-ribose. When L-ribose was modeled to be liganded to the active site metal M1 (magnesium) by oxygens O2 and O4 (analogously to D-xylose), the O4 atom of the substrate detached quickly from the metal M1 during the simulation, even though the charge of M1 was set to +2.0. On the contrary, when D-xylose was modeled to be liganded to M1, the substrate did not move away from its place during the simulation with similar parameters. Furthermore, the oxygen O1 was quite far away from the metal M2 when compared to D-xylose and when the catalytic metal M2 was modeled to be in the same position as in 6XIM and the oxygens O1 and O2 were modeled to be in the reactive *cis*-conformation.

The crystal structures of XI with D-xylose show that O2 and O4 of the substrate are liganded to the metal M1. It appeared from our simulations that the mutation V135N increases the reaction rate with L-ribose by keeping the substrate better in a conformation in which O4 is liganded to the metal M1. Hydrogen bonding between Asn introduced into the position 135 and Glu-181 moved the side chain of Glu-181 about 0.3 Å towards Asn at position 135. This modification of the active site may be involved in the stabilization of L-ribose in a conformation in which the liganding of O4 to the metal M1 is improved. An altered K_m value was the main factor behind the improved reaction rate due to mutation V135. Thus, it appears that the better contact between the O4 atom of L-ribose and the structural metal M1 is a key factor in the improved K_m value of the V135N mutant. The simulations suggested that the longer distance of the substrate atoms C2 and C1 to the catalytic metal M2 in L-ribose compared to D-xylose is another reason for the lowered reaction rate in the enzyme catalysis by XI. The mutation V135N shortened these distances slightly for L-ribose.

The finding that the mutation V135N decreased the reaction with D-xylose by only 20% but over 75% with D-glucose indicates that the size of the substrate determines how the mutation V135N affects the enzyme reaction. Also, the reaction rate with L-arabinose was about the same with the wild type and the V135N mutant, showing that pentoses are not necessarily negatively affected by the mutation V135N. When the mutation V135N was modeled to XI structure, Asn-135 does not appear to form a hydrogen bond to D-xylose in 6XIM, whereas a hydrogen bond can be formed to D-sorbitol (mimicking D-glucose) in 5XIM (crystal structure of *A. missouriensis* XI with D-sorbitol). The reaction with D-xylose showed that the potential hydrogen bonding of Asn-135 to the Glu-181 side chain carbonyl oxygen does not have any major effect on the enzyme catalysis. Therefore, the potential hydrogen bonding of Asn-135 to D-glucose in the *A. missouriensis* XI mutant V135N is a likely reason for the decreased reaction rate with D-glucose. However, the mutation V135N improved the K_m, thus indicating that D-glucose binds better to the active site probably due to the hydrogen bonding between Asn-135 and C6–OH. Product release could then be lowered as a consequence.

Mutations at the position 135 or corresponding site have been reported either to decrease or increase the reaction rate of XI [39,40]. Our results for *A. missouriensis* XI suggested that increased hydrogen bonding near the O5–O6 region of the substrate is not necessarily beneficial for the enzyme reaction, except when the hydrogen bond improves the conformation and interactions of a non-natural substrate in the active site.

Acknowledgements

We thank Johanna Aura for technical assistance. Support from the Academy of Finland, the National Technology Agency of Finland, TEKES, and the Research Foundation of Helsinki University of Technology is gratefully acknowledged. CSC, the Finnish IT center for science, is acknowledged for computer resources.

References

[1] B. Asbóth, G. Náray-Szabó, Mechanism of action of D-xylose isomerase, Curr. Protein Pept. Sci. 1 (2000) 237–254.
[2] H. Häusler, A.E. Stütz, D-xylose (D-glucose) isomerase and related enzymes in carbohydrate synthesis, Top. Curr. Chem. 215 (2001) 77–114.
[3] A. Vuolanto, O. Pastinen, H.E. Schoemaker, M. Leisola, C-2 epimer formation of tetrose, pentose and hexose sugars by xylose isomerase, Biocatal. Biotransform. 20 (2002) 235–240.

[4] Y.B. Tewari, R.N. Goldberg, An investigation of the equilibria between aqueous ribose, ribulose and arabinose, Biophys. Chem. 22 (1985) 197–204.
[5] O. Pastinen, H.E. Schoemaker, M. Leisola, Xylose isomerase catalysed novel hexose epimerization, Biocatal. Biotransform. 17 (1999) 393–400.
[6] O. Pastinen, K. Visuri, H.E. Schoemaker, M. Leisola, Novel reactions of xylose isomerase from *Streptomyces rubiginosus*, Enzyme Microb. Technol. 25 (1999) 695–700.
[7] M. Garcia-Viloca, C. Alhambra, A.G. Truhlar, J. Gao, Hydride transfer catalyzed by xylose isomerase: mechanism and quantum effects, J. Comput. Chem. 24 (2003) 177–190.
[8] T.D. Fenn, D. Ringe, G.A. Petsko, Xylose isomerase in substrate and inhibitor Michaelis states: atomic resolution studies of a metal-mediated hydride shift, Biochemistry 43 (2004) 6464–6474.
[9] A.-M. Lambeir, I. Lasters, W.J. Quax, J.M. Van der Laan, Protein engineering of xylose (glucose) isomerase from *Actinoplanes missouriensis*: 2. Site-directed mutagenesis of xylose binding site, Biochemistry 31 (1992) 5459–5466.
[10] R.D. Whitaker, Y. Cho, J. Cha, H.L. Carrell, J.P. Glusker, P.A. Karplus, C.A. Batt, Probing roles of active site residues in D-xylose isomerase, J. Biol. Chem. 270 (1995) 22895–22906.
[11] H. Hu, Y.Y. Shi, C.X. Wang, Exploring the interaction between D-xylose isomerase and D-xylose by free energy calculation, Proteins 26 (1996) 157–166.
[12] M. Whitlow, A.J. Howard, B.C. Finzel, T.L. Poulos, E. Winborne, G.L. Gilliland, A metal-mediated hydride shift mechanism for xylose isomerase based on the 1.6 Å *Streptomyces rubiginosus* structures with xylitol and D-xylose, Proteins 9 (1991) 153–173.
[13] O. Turunen, K. Etuaho, F. Fenel, J. Vehmaanperä, X. Wu, J. Rouvinen, M. Leisola, Combination of weakly stabilizing mutations with a disulfide-bridge in the α-helix region of *Trichoderma reesei* endo-1,4-β-xylanase II increases the thermal stability through synergism, J. Biotechnol. 88 (2001) 37–46.
[14] N. Guex, M.C. Peitsch, SWISS-MODEL and the Swiss-PdbViewer: an environment for comparative protein modeling, Electrophoresis 18 (1997) 2714–2723.
[15] M.M. Bradford, A rapid and sensitive method for the quantitation of microgram quantities of protein utilising the principle of protein-dye binding, Anal. Biochem. 72 (1976) 248–254.
[16] P. Kuzmic, Program DYNAFIT for the analysis of enzyme kinetic data: application to HIV proteinase, Anal. Biochem. 237 (1996) 260–273.
[17] QUANTA Accelrys Incorporation, San Diego, CA, USA.
[18] J. Jenkins, J. Janin, F. Rey, M. Chiadmi, H. van Tilbeurgh, I. Lasters, M. De Maeyer, D. Van Belle, S.J. Wodak, M. Lauwereys, P. Stanssens, N.T. Mrabet, J. Snauwaert, G. Matthyssens, A.-M. Lambeir, Protein engineering of xylose (glucose) isomerase from *Actinoplanes missouriensis*: 1. Crystallography and site-directed mutagenesis of metal binding sites, Biochemistry 31 (1992) 5449–5458.
[19] C.L. Brooks, M. Karplus, Deformable stochastic boundaries in molecular dynamics, J. Chem. Phys. 79 (1983) 6312–6325.
[20] E.Y. Lau, T.C. Bruice, Active site dynamics of the *Hha*I methyltransferase: insights from computer simulation, J. Mol. Biol. 293 (1999) 9–18.
[21] B.R. Brooks, R.E. Bruccoleri, B.D. Olafson, D.J. States, D. Swaminathan, M. Karplus, CHARMM: a program for macromolecular energy, minimization and dynamics calculations, J. Comp. Chem. 4 (1983) 187–217.
[22] F.A. Momany, R. Rone, Validation of the general purpose Quanta 3.2/CHARMm force field, J. Comp. Chem. 13 (1992) 888–900.
[23] A.T. Brünger, M. Karplus, Polar hydrogen positions in proteins: empirical energy placements and neutron diffraction comparison, Proteins 4 (1988) 148–156.
[24] W.L. Jorgensen, J. Chandrasekhar, J. Madura, R.W. Impey, M.L. Klein, Comparison of simple potential functions for simulating liquid water, J. Chem. Phys. 97 (1983) 926–935.
[25] J.-P. Ryckaert, G. Cicotti, H.J.C. Berendsen, Numerical integration of the cartesian equations of motion for a system with constraints: molecular dynamics on *n*-alkanes, J. Comp. Physiol. 23 (1977) 327–341.
[26] P.J. Steinbach, B.R. Brooks, New spherical-cutoff methods for long-range forces in macromolecular simulation, J. Comp. Chem. 15 (1994) 667–683.
[27] http://comp.chem.umn.edu.
[28] A. Warshel, M. Levitt, Theroretical studies of enzymic reactions: dielectric, electrostatic, and steric stabilization of the carbonium ion in the reaction of lysozyme, J. Mol. Biol. 103 (1976) 227–249.
[29] J.J.P. Stewart, Optimization of parameters for semiempirical methods, J. Comp. Chem. 10 (1989) 209–220.
[30] R.S. Mulliken, Electronic population analysis on LCAO-MO molecular wave function, J. Chem. Phys. 23 (1955) 1833–1840.
[31] G. Vriend, WHAT IF: a molecular modeling and drug design program, J. Mol. Graph. 8 (1990) 52–56.
[32] J. Nielsen, G. Vriend, Optimizing the hydrogen-bond network in Poisson–Boltzmann equation-based p*K*a calculations, Proteins: Struct., Funct., Genet. 43 (2001) 403–412.
[33] J. KarimûÊki, T. Parkkinen, H. Santa, O. Pastinen, M. Leisola, J. Rouvinen, O. Turunen, Engineering the substrate specificity of xylose isomerase, Protein Eng. Des. Sel. 17 (2004) 861–869.
[34] A.D. Becke, Density-functional exchange-energy approximation with correct asymptotic-behavior, Phys. Rev., A 38 (1988) 3098–3100.
[35] C. Lee, W. Yang, R.G. Parr, Development of the Colle–Salvetti correlation-energy formula into a functional of the electron-density, Phys. Rev., B 37 (1998) 785–789.
[36] R. Ahlrichs, M. Bär, M. Häser, H. Horn, C. Kölmel, Electronic-structure calculations on workstation computers—the program system TURBOMOLE, Chem. Phys. Lett. 162 (1989) 165–169.
[37] K. Eichkorn, O. Treutler, H. Öhm, M. Häser, R. Ahlrichs, Auxiliary basis-sets to approximate coulomb potentials, Chem. Phys. Lett. 242 (1995) 652–660.
[38] R.T. Sanderson, An interpretation of bond lengths and a classification of bonds, Science 114 (1951) 670–672.
[39] M. Meng, C. Lee, M. Bagdasarian, J.G. Zeikus, Switching substrate preference of thermophilic xylose isomerase from D-xylose to D-glucose by redesigning the substrate binding pocket, Proc. Natl. Acad. Sci. U. S. A. 88 (1991) 4015–4019.
[40] A.-M. Lambeir, I. Lasters, W.J. Quax, J.M. Van den Laar, Glucose isomerases having altered substrate specificity. US Patent 5,310,665 (1994).